International Journal of Rotating Machinery
1999, Vol. 5, No. 4, pp. 241–250
Reprints available directly from the publisher
Photocopying permitted by license only

Performance Evaluation of an Air-Conditioning Compressor Part II: Volute Flow Predictions*

YU-TAI LEE† and THOMAS W. BEIN

David Taylor Model Basin, 9500 MacArthur Blvd., West Bethesda, MD 20817-5700, USA

(Received 12 May 1998; In final form 10 July 1998)

A numerical method that solves the Reynolds-averaged Navier–Stokes equations is used to study an inefficient component of a shipboard air-conditioning HCFC-124 compressor system. This high-loss component of the centrifugal compressor was identified as the volute through a series of measurements given in Part I of the paper. The predictions were made using three grid topologies. The first grid closes the connection between the cutwater and the discharge diffuser. The other two grids connect the cutwater area with the discharge diffuser. Experiments were performed to simulate both the cutwater conditions used in the predictions. Surface pressures along the outer wall and near the inlet of the volute were surveyed for comparisons with the predictions. Good agreements between the predicted results and the measurements validate the calculations. Total pressure distributions and flow stream traces from the prediction results support the loss distribution through the volute. A modified volute configuration is examined numerically for further loss comparison.

Keywords: Air-conditioning compressor, Volute, Cutwater (tongue), Diffuser, Reynolds-averaged Navier–Stokes equations

INTRODUCTION

U.S. Navy shipboard centrifugal chilled water air-conditioning systems currently utilize refrigerant CFC-114. In response to the world community decision to eliminate the use of CFC refrigerants, the U.S. Navy has begun a program to convert the air conditioning plants to an environmentally acceptable refrigerant. HCFC-124 was identified as a potential candidate to replace the CFC-114. A generic centrifugal compressor unit, as shown in Fig. 1, was designed based on the properties of the HCFC-124. The compressor consists of two rows of inlet guide vanes, an impeller, a vaneless diffuser, an elbow, and a volute and its discharge diffuser. The isentropic efficiency of the new compressor was measured to be 10% lower than the design prediction. A detailed measurement of the systems component performance, as shown in Bein and Lee (1998), indicated that the volute

* This paper was originally presented at ISROMAC-7.

† Corresponding author. Tel.: 301 227 1328. Fax: 301 227 5707. E-mail: ylee@dt.navy.mil.

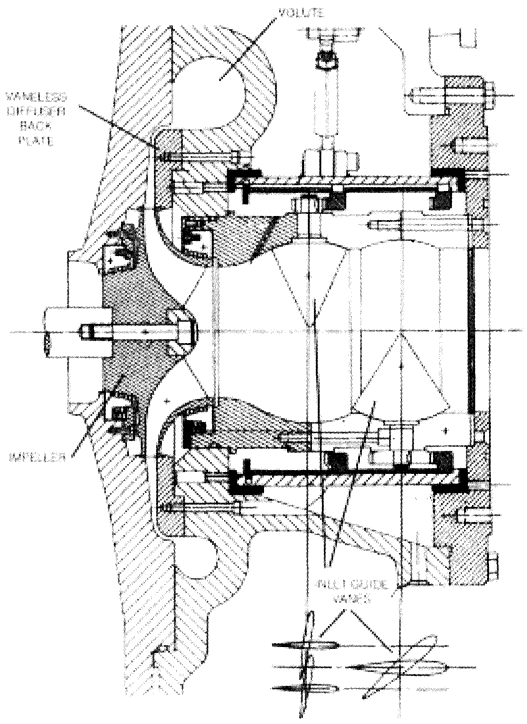

FIGURE 1 Generic compressor unit for shipboard air-conditioning system.

contains the largest area of loss in the compressor. Thus, a computational analysis was made to investigate the loss in the volute.

Limited studies (Iversen *et al.*, 1960; Stiefel, 1972; Brownell and Flack, 1985; Van Den Braembussche and Hande, 1990; Elholm *et al.*, 1992; Ayder *et al.*, 1993; Ayder and Van Den Braembussche, 1991; 1994) were performed for the volute flow and its interaction with other rotating and non-rotating components of centrifugal compressors. Most of these works concentrated on the experimental studies. A recent study by Ayder and Van Den Braembussche (1994) used an Euler solver to examine the volute flow. They implemented a loss model in the code to account for the friction losses. The current numerical model solves Reynolds-averaged Navier–Stokes equations. In the following sections, the experimental facility used to record the volute flow characteristics and the measured quantities are first introduced. A brief review of the current numerical method follows. For the numerical results, three different gridding approaches are examined and the predicted pressure distributions are compared with the experimental data. The flow region with a high loss is identified from total pressure distributions. A modified volute configuration is studied based on the present numerical model to evaluate the effect of flow recirculation downstream of the cutwater region.

EXPERIMENTAL SETUP

In order to provide detailed information for understanding the compressor performance shown in Fig. 1, an experimental setup using the Centrifugal Compressor Development Facility at the Annapolis Laboratory of the David Taylor Model Basin was established. There are two rows of inlet guide vanes. The shrouded impeller has 13 main blades and 13 splitter blades with a 30° backswept. At the design point, the impeller rotates at 17,983 rpm with a tip speed of 630 fps (192 m/s). The impeller exit radius is 4.02 in (102.11 mm). The radius ratio of the vaneless diffuser exit to the impeller exit is 1.52. The inlet width of the vaneless diffuser is 0.35 in (8.89 mm) and the exit width is 0.1425 in (3.62 mm). The flow coefficient is 0.0654 and the head coefficient is 1.2324. The specific speed is 0.0903 (which is calculated using rpm, cfs, and enthalpy difference). A total of 40 static pressure taps were installed along the front plate and the back plate of the compressor in the vaneless diffuser and the volute sections. They are distributed along the complete volute flow passage with a concentration of pressure taps at the cutwater. In addition, five total pressure probes were installed to measure velocities at the exit of the vaneless diffuser, inside the volute immediately downstream of the cutwater, in the middle of the volute, and at the exit of the discharge diffuser. Three dynamic pressure transducers were installed in the vaneless diffuser and one in the volute to measure the dynamic pressure response. The estimated error for the static

pressure measurements is 2%. The details of the measurement setup are shown in Bein and Lee (1998a,b).

For evaluating the effect of the flow through the volute, the measurements were carried out in two steps. A flush mounted movable cutwater plug was installed near the cutwater. This plug, when pushed out from outside of the back plate, was designed to block the fluid flowing back to the cutwater from the discharge diffuser. The experimental condition was adjusted to the compressor design condition.

Three sets of pressure data were taken from each pressure probe. The steady static pressures, referred to as the data of the open cutwater, were obtained by averaging these three data sets. Under the same conditions, a second set of measurements was performed for the closed cutwater. The second series is referred to as the data of the closed cutwater. The measured isentropic efficiency of the closed cutwater condition drops 0.5% when compared with the open cutwater condition as shown in Bein and Lee (1998a,b).

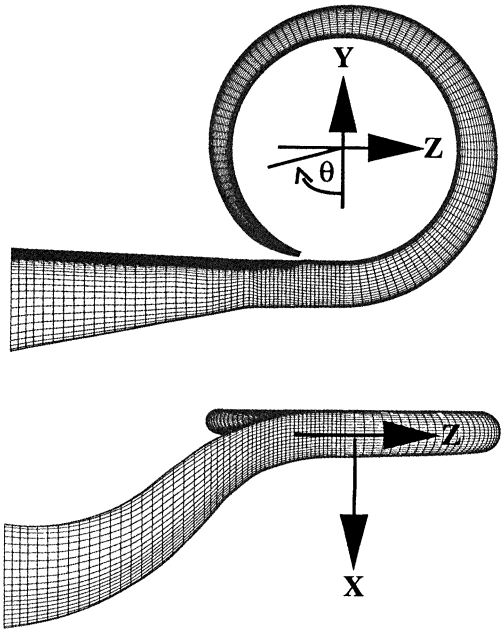

FIGURE 2 Volute configuration and coordinate system.

COMPUTATIONAL METHOD

Governing equations, including the continuity, momentum and energy equations, for compressible flows are solved with a two-equation k-ε turbulence model for the volute flow. The coordinate for depicting the volute geometry is shown in Fig. 2. The governing equations in curvilinear coordinates are written as:

$$\frac{1}{J}\frac{\partial}{\partial t}(pq) = \frac{\partial}{\partial \xi_i}\left(\rho U_i q + \mu_{\text{eff}} G_{ij}\frac{\partial q}{\partial \xi_i}\right) + S_{\text{q}} \qquad (1)$$

where $q = [1, u_x, u_y, u_z, h, k, \varepsilon]$ and ρ, J, U_i, G_{ij} represent fluid density, the Jacobian of the coordinate transformation, transformed velocities, and diffusion metrics, respectively. The effective viscosity μ_{eff} represents a sum of the laminar viscosity μ and the turbulent eddy viscosity μ_{t} then re-scaled by a turbulence Prandtl number or Schmidt number σ_{q}. The turbulent eddy viscosity $\mu_{\text{t}} = \rho C_\mu k^2/\varepsilon$ and $C_\mu = 0.09$. The source term in Eq. (1) is

$$S_{\text{q}} = \frac{1}{J}\begin{bmatrix} 0 \\ -p_{xi} + \nabla[\mu_{\text{eff}}(u_j)_{xi}] - \frac{2}{3}(\mu_{\text{eff}}\nabla u_j)_{xi} \\ \dfrac{\text{D}p}{\text{D}t} + \Phi \\ \rho(P_{\text{r}} - \varepsilon) \\ \rho(\varepsilon/k)[(C_1 + C_3(P_{\text{r}}/\varepsilon))P_{\text{r}} - C_2\varepsilon] \end{bmatrix} \qquad (2)$$

and P_{r} stands for the turbulence kinetic energy production rate. The constants for the ε-equation are $C_1 = 1.15$, $C_2 = 1.90$ and $C_3 = 0.25$.

Finite-difference approximations are used to discretize the transport equations on non-staggered grid mesh systems. A second-order upwind scheme is used to model the convective terms and second-order central difference schemes are used for the viscous and source terms of Eqs. (1) and (2). For turbulence quantities, the convection process is modeled by a first-order upwind scheme. A pressure based predictor/corrector solution procedure shown in Chen (1989) is employed to achieve velocity-pressure coupling. The discretized systems are solved by an implicit Euler time-marching scheme.

The numerical solutions were considered converged when the residuals of each discretized equation drop five orders of magnitude.

PREDICTION FOR CLOSED CUTWATER

For the flow past the vaneless diffuser and the elbow, both calculations and the experimental data indicated that flow past the vaneless diffuser is completely mixed out before reaching the 90-degree elbow. Thus, the inflow condition for the present calculations to the volute after the elbow was assumed to be uniform initially along the meridional direction. The swirl component of the inlet velocity was taken from the measured value. As the time-marching scheme proceeded the total mass flow through the volute inlet was maintained at the design condition. It is worth noting that the uniform-flow assumption was used in the conventional volute design theory described by Traupel (1977) and by Eckert and Schnell (1980). The measured static pressure at exit plane of the discharge diffuser was used as the exit boundary condition. In order to account for the real gas properties (HCFC-124) the computation was performed using the perfect gas law with an isentropic exponent for the real gas.

An O-grid topology, shown in Fig. 3, at each volute cross section was first used to study the flow pattern. The grid contains 151 meridional nodes and 75×25 nodes at each cross plane. This grid system has a singular line at the center of the volute cross section. This singular line prevents the generalization of the grid transition in the cutwater region for connecting with the discharge diffuser.

The predicted pressure distributions at the volute inlet and at the wall of mid-radius are compared in Fig. 4 with the measured distributions for the closed cutwater case. The labeled "EXP (INLET)" pressure is the measured pressure at the vaneless diffuser exit. The cutwater region starts at $\theta = 22.5°$ where the measured minimum pressure occurs. The computational grid starts at $\theta = 25°$. Since the cutwater was not connected, the pressure recovery at smaller volute angles was not predicted. The predictions agree well with the measurements at the inlet and the wall locations. Both the prediction and the measurement, however, show differences between the inlet and the wall pressures. Figure 5 shows a calculated pressure contour plot over a typical cross section (e.g. $\theta = 145°$) along the

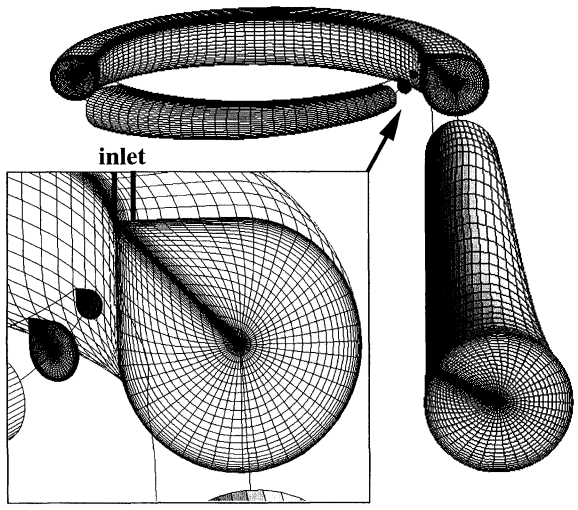

FIGURE 3 The O-grid structure for the closed cutwater volute.

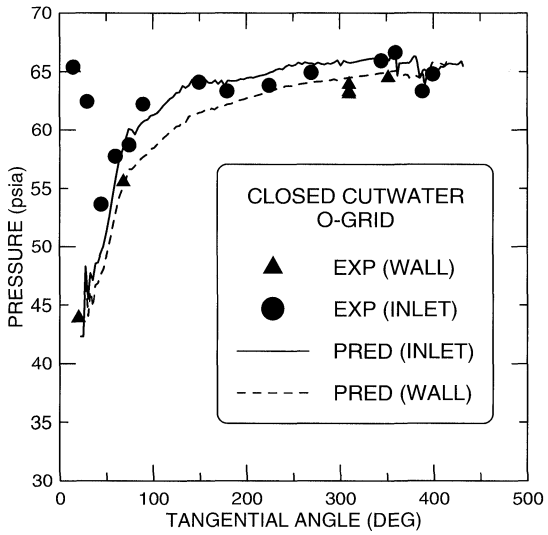

FIGURE 4 Comparison of static pressure for the closed cutwater volute.

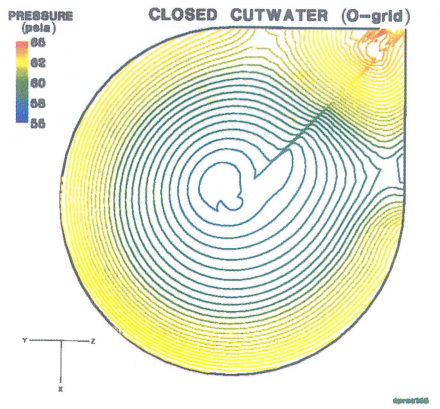

FIGURE 5 Predicted static pressure contours at $\theta = 145°$ O-grid for closed cutwater. (See Color Plate I at the back of this issue.)

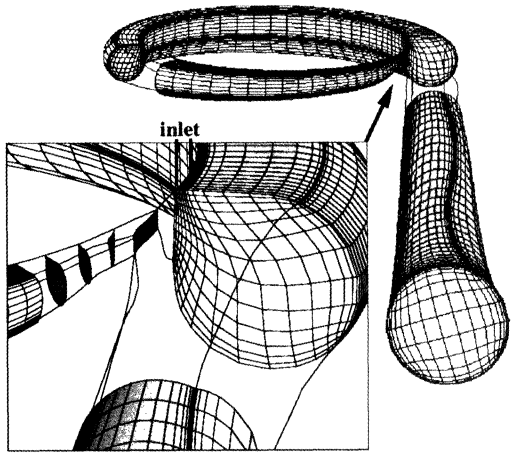

FIGURE 6 The H-grid one-block topology for using open cutwater volute.

volute pass. The pressure distribution is uniformly distributed on the left side of the figure, i.e. larger radius wall. There is a pressure gradient between the inlet and the bottom wall as it is shown in Fig. 4. In addition, the results indicated that the sharp suction pressure near the cutwater was not produced by the returning flow from the discharge diffuser through the cutwater. This result also confirms the small measured difference in efficiency between the closed and open cutwater cases.

PREDICTION FOR OPEN CUTWATER

In order to connect the cutwater with the discharge diffuser, the O-grid topology was changed to an H-grid. In Fig. 6, the H-grid is a one block structured grid and has 162 nodes in the meridional direction, 18×14 nodes on each cross plane of the volute pass. Since the inlet portion of the grid is relatively finer than the other parts, the gridlines are very skew near the inlet. The overall grid distribution is coarse because of the restriction of the grid skewness. Similar boundary conditions were applied except an interface boundary was used at the connecting plane of the cutwater between the volute and the discharge diffuser. The predicted inlet and wall pressures shown in Fig. 7 show that the variation

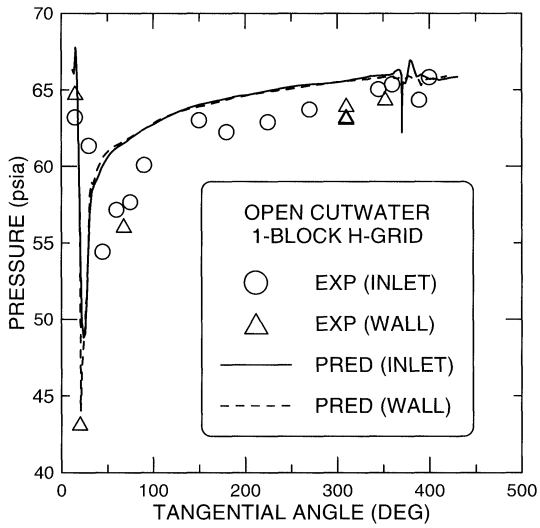

FIGURE 7 Comparison of static pressure for open cutwater volute using one-block grid.

in pressure across each cross section is small. Although the predicted low pressure near the cutwater agrees well with the open-cutwater measurement, the calculated results overpredict the measured pressures in the other volute sections.

A two-block grid structure was generated to reduce the grid skewness of the one-block approach. Figure 8 shows the 2-block grid structure. The first block contains the inlet portion and

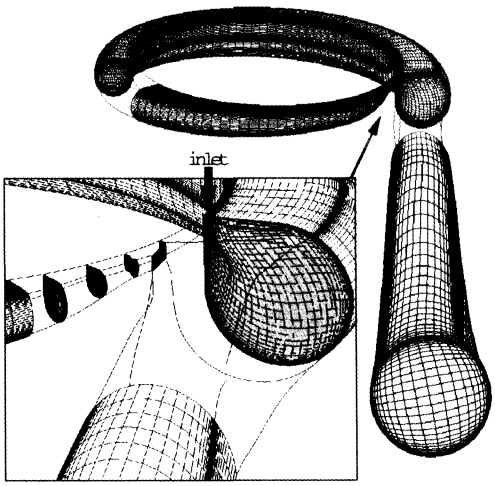

FIGURE 8 The H-grid two-block topology for open cutwater volute.

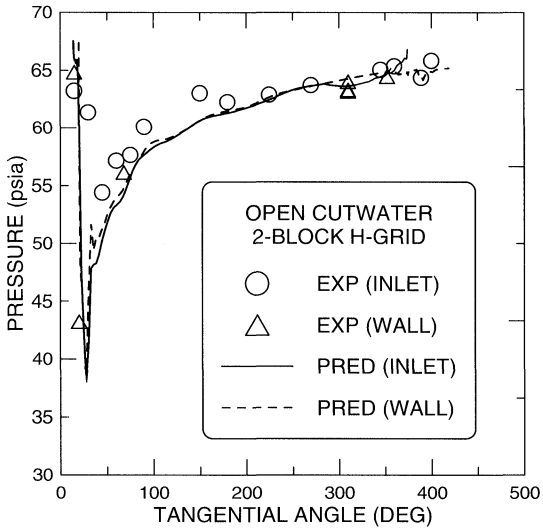

FIGURE 9 Comparison of static pressures for open cutwater volute using two-block grid.

consists of $119 \times 21 \times 47$ nodes and the second block has $201 \times 35 \times 47$ nodes. The grid nodes at each cross-section are more than quadrupled. The predicted pressure is compared with the measurement in Fig. 9. The agreement between the calculation and the measurement is better than the one-block approach due to the grid resolution and grid distribution. Figure 10 shows the predicted

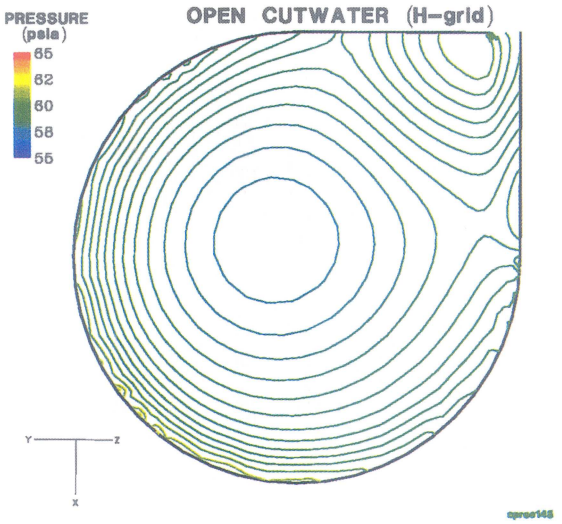

FIGURE 10 Predicted static pressure contours at $\theta = 145°$ using two-block grid for open cutwater. (See Color Plate II at the back of this issue.)

pressure contours for the open cutwater condition at the same section as Fig. 5 shows. The general feature is similar between Figs. 5 and 10 except the overall pressure levels. Due to the opening of the cutwater, the inlet pressure and its gradient between the inlet and the wall are lower than the closed cutwater case. Both cases from the experiment and the calculation, however, show that the low pressure occurs near the cutwater.

Figure 11 shows a combined plot for the open and the closed cutwater conditions from both measurements and predictions. Unfilled symbols used in Fig. 11 are for the open cutwater and filled symbols are for the closed cutwater. It is shown clearly from calculations and measurements that the inlet pressure is consistently lower for the open case than for the closed case. The wall pressure, however, remains similar. The measured data shows that the pressure for the open cutwater condition is about 2–4% lower than that for the closed cutwater condition at the inlet and the difference is less than 2% at the wall. Although both the measurement and the prediction show lower peak pressures for the open cutwater case at the design condition, the peak low pressure near the cutwater is independent of whether the cutwater is

open or closed. This matches with the efficiency measured results between the two conditions.

Figure 12 shows the predicted total pressure contours at six cross-sections. The total pressure contours shown indicate that a large loss occurs downstream of the cutwater and at the opposite side of the inlet on the plane of the volute sections ($\theta = 35.5°$ and $\theta = 53.5°$). The flow of this mixing area (between $\theta = 30°$ and $\theta = 60°$) originates from the inflow at the cutwater as shown in Fig. 12. This flow mixing and the recirculation cause the loss and low pressure which is independent of the cutwater conditions for the returning flow from the discharge diffuser.

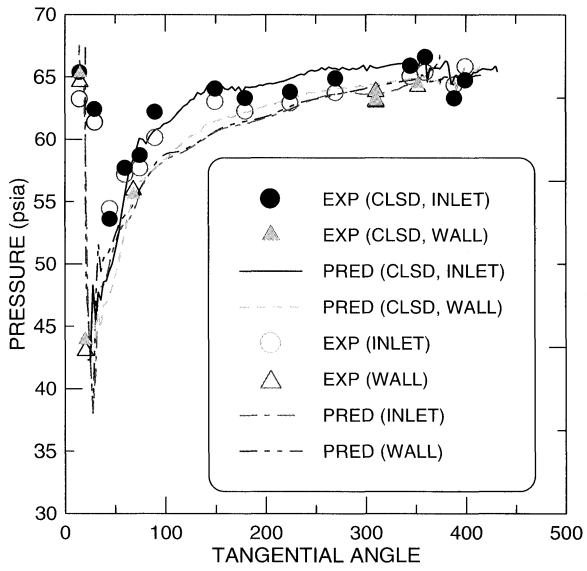

FIGURE 11 Composite plot of Figs. 4 and 9.

A MODIFIED SHAPE IN THE MIXING AREA

Since the flow recirculation region occupied the bottom portion of the cross section downstream of the cutwater, a modified volute shape from $\theta = 27°$ to $\theta = 125°$ was examined. Figure 13 shows the difference between the original and the modified shapes at $\theta = 56°$. Transition of the cross-sectional shape was smoothly changed. Figure 14 shows the difference in calculated pressures along the volute wall. The peak suction pressure at the cutwater increases slightly, but the pressure recovery through the rest of the volute increases. The volute exit

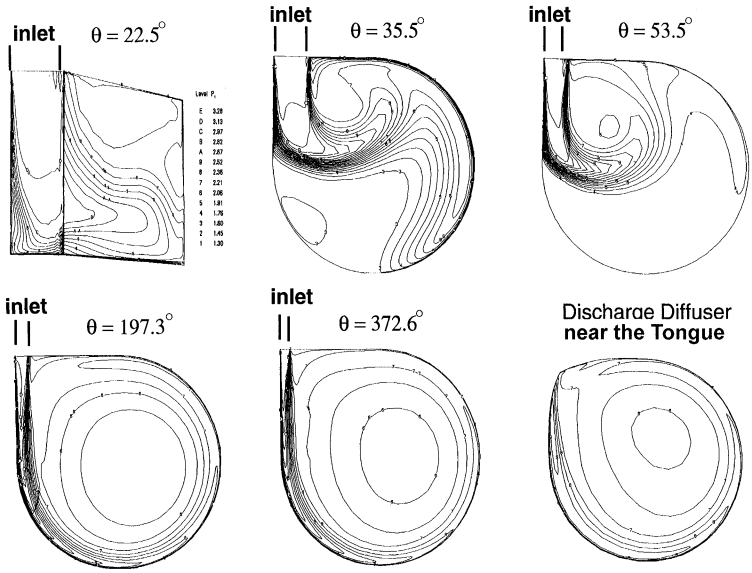

FIGURE 12 Comparison of static pressures for open cutwater volute using two-block grid.

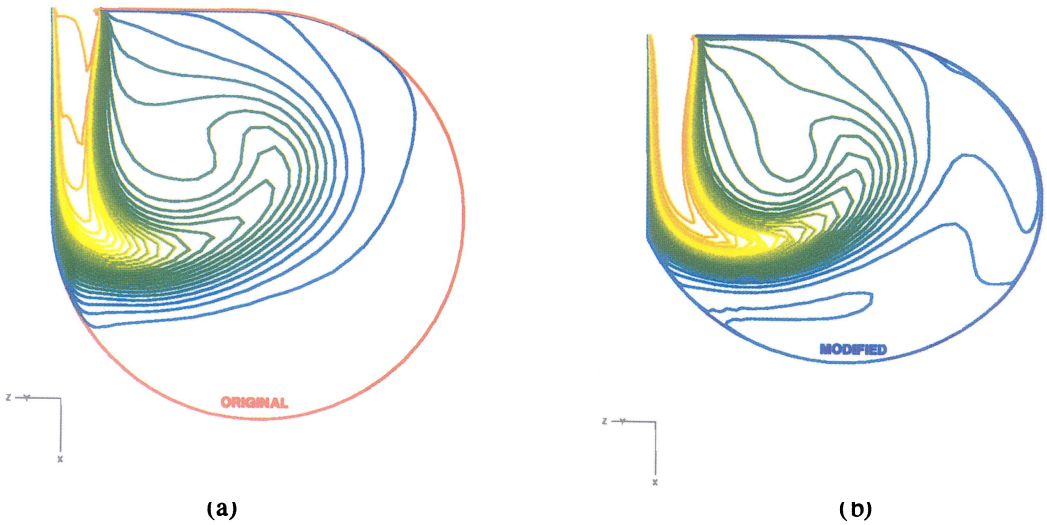

FIGURE 13 Predicted total pressure contours at $\theta = 56°$ for (a) original (b) modified volute cross sections. (See Color Plate III at the back of this issue.)

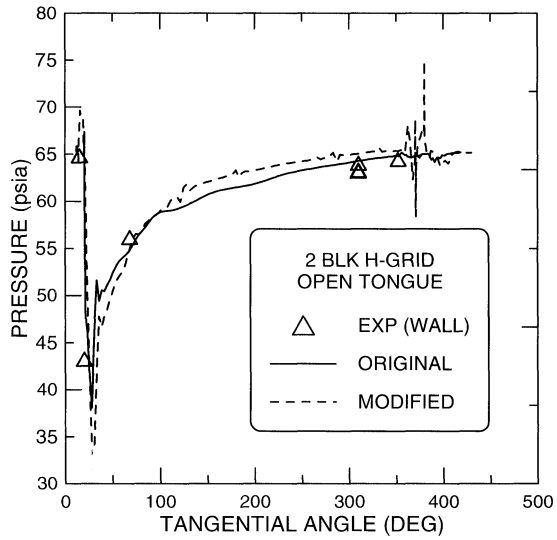

FIGURE 14 Comparison of predicted wall static pressure for original and modified volute cross sections.

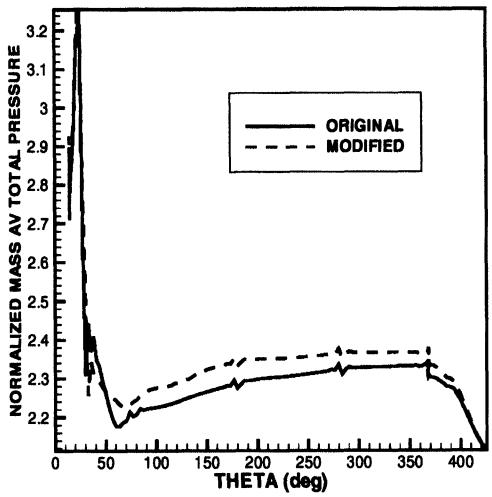

FIGURE 15 Distributions of mass averaged total pressure along volute pass for original and modified volute cross sections.

pressure, however, was not changed due to prescribing the same exit pressure during the calculation. Figure 15 shows the mass-averaged total pressure on each cross section along the volute pass for both the original and the modified cross sections. The modified shape produces slightly larger loss at the cutwater. The loss that occurs in the other part of the volute decreases, although it remains the same at the exit due to the prescribed boundary condition.

CONCLUSIONS

A numerical method that solves the Reynolds-averaged Navier–Stokes equations was used to study the volute flow of a shipboard air conditioning compressor system. The predictions were made using three grid topologies. The first grid closes the connection of the cutwater region with the discharge diffuser. The other two grids connect the cutwater area with the discharge diffuser. Experiments were performed to simulate both the cutwater conditions used in the predictions. Good agreements between the predicted results and the measurements validate the calculations. The comparison between the prediction results and measurements indicates that (i) the low pressure and the large loss at the cutwater are not related to the volute returning flow through the cutwater and are related to the inlet flow at the cutwater from the vaneless diffuser and the cutwater's specific geometry; (ii) the loss occurs downstream of the cutwater due to flow mixing and recirculation and is improved by reshaping the cross section; (iii) when the cutwater is closed, the pressure gradient that existed between the inlet and the wall is larger than the open cutwater case, and so is the secondary loss; (iv) the conventional cutwater design at the operating condition has an adverse contribution in pressure recovery due to the low-pressure peak produced at the cutwater.

Acknowledgments

This work was supported by the Chief of Naval Operstions under the Shipboard Energy Conservation Program. The program monitors are Mr. H. Hodgkins of OPNAV N420C and Mr. W. Stoffel of NSWC Code 8590. Partial computational resource was given by the DoD Major Shared Resource Center of the Naval Oceanographic Office at Stennis Space Center, Mississippi. Special thanks are due to Mr. M. Tse of the Vector Research Division of the A&T Engineering Technologies for his preparation of several figures shown in this paper.

NOMENCLATURE

$C_{1,2,3,\mu}$	turbulence model constants
G_{ij}	$1/J\,\partial\xi_i/\partial x_k\,\partial\xi_j/\partial x_k$
h	enthalphy
J	Jacobian, $\partial(\xi,\eta,\zeta)/\partial(x,y,z)$
k	turbulent kinetic energy
p	static pressure
P_r	production rate of k
P_t	total pressure
q	vector of dependent variables in Eq. (1)
S_q	source terms
t	time
u_j	i-component velocity
U_i	$u_j/J\,\partial\xi_i/\partial x_j$
x,y,z	Cartesian coordinates
ε	turbulent dissipation
Φ	diffusion terms in energy equation
μ	laminar viscosity
μ_{eff}	effective viscosity $(\mu+\mu_t)/\sigma_q$
μ_t	turbulent eddy viscosity
θ	volute tangential angle
ρ	fluid density
σ_q	turbulent Prandtl or Schmidt number
ξ_i	transformed coordinates, i.e. ξ, η, ζ

References

Ayder, E. and Van Den Braembussche, R.A. (1991) Experimental study of the swirling flow in the internal volute of a centrifugal compressor, *ASME Paper No. 91-GT-7.*

Ayder, E., Van Den Braembussche, R.A. and Brasz, J.J. (1993) Experimental and theoretical analysis of the flow in a centrifugal compressor volute, *ASME Journal of Turbomachinery*, **115**, 582–589.

Ayder, E. and Van Den Braembussche, R.A. (1994) Numerical analysis of the three-dimensional swirling flow in centrifugal compressor volutes, *ASME Journal of Turbomachinery*, **116**, 462–468.

Bein, T.W. and Lee, Y.T. (1998a) Performance evaluation of 125 ton HCFC-124 centrifugal compressor, *Carderock Division, Naval Surface Warfare Center, Report CARDIVNSWC-TR-82-98/08.*

Bein, T.W. and Lee, Y.T. (1998b) Performance evaluation of an air-conditioning compressor. Part I: Measurement and design modeling, *ISROMAC-7, Proc. the 7th International Symposium on Transport Phenomena and Dynamics of Rotating Machinery*, Vol. C, pp. 1624–1633.

Brownell, R.B. and Flack, R.D. (1985) Flow characteristics in the volute and tongue region of a centrifugal pump, *ASME Paper No. 85-GT-82.*

Chen, Y.S. (1989) Compressible and incompressible flow computations with a pressure based method, *AIAA 89-0286, 27th Aerospace Science Meeting*.

Eckert, B. and Schnell, E. (1980) *Axial- und Radialkompressoren*, 2nd ed., Springer-Verlag.

Elholm, T., Ayder, E. and Van Den Braembussche, R.A. (1992) Experimental study of the swirling flow in the volute of a centrifugal pump, *ASME Journal of Turbomachinery*, **114**, 366–372.

Iversen, N., Rolling, R. and Carlson, J. (1960) Volute pressure distribution, radial force on the impeller, and volute mising losses of a radial flow centrifugal pump, *ASME Journal of Turbomachinery*, **82**(2), 120–126.

Stiefel, W.L. (1972) Experiences in the development of radial compressors, *Lecture Notes for Advanced Radial Compressor Course* held at von Karman Institute, Brussels.

Traupel, W. (1977) *Thermische Turbomaschinen*, 3 ed., Springer-Verlag.

Van Den Braembussche, R.A. and Hande, B.M. (1990) Experimental and theoretical study of the swirling flow in centrifugal compressor volutes, *ASME Journal of Turbomachinery*, **112**, 38–43.

MANEY
publishing

The Institute of Materials, Minerals & Mining

ENERGY MATERIALS

NEW FOR 2006

Materials Science & Engineering for Energy Systems

Maney Publishing on behalf of the Institute of Materials, Minerals and Mining

Economic and environmental factors are creating ever greater pressures for the efficient generation, transmission and use of energy. Materials developments are crucial to progress in all these areas: to innovation in design; to extending lifetime and maintenance intervals; and to successful operation in more demanding environments. Drawing together the broad community with interests in these areas, *Energy Materials* addresses materials needs in future energy generation, transmission, utilisation, conservation and storage. The journal covers thermal generation and gas turbines; renewable power (wind, wave, tidal, hydro, solar and geothermal); fuel cells (low and high temperature); materials issues relevant to biomass and biotechnology; nuclear power generation (fission and fusion); hydrogen generation and storage in the context of the 'hydrogen economy'; and the transmission and storage of the energy produced.

As well as publishing high-quality peer-reviewed research, *Energy Materials* promotes discussion of issues common to all sectors, through commissioned reviews and commentaries. The journal includes coverage of energy economics and policy, and broader social issues, since the political and legislative context influence research and investment decisions.

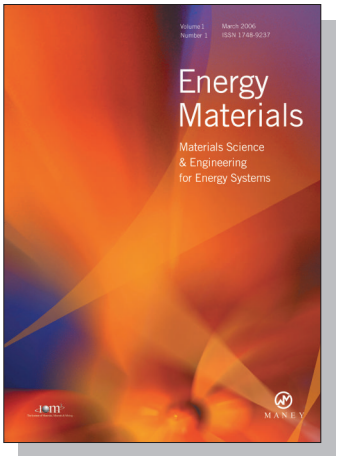

CALL FOR PAPERS

Contributions to the journal should be submitted online at **http://ema.edmgr.com**

To view the Notes for Contributors please visit: **www.maney.co.uk/journals/notes/ema**

Upon publication in 2006, this journal will be available via the Ingenta Connect journals service. To view free sample content online visit: **www.ingentaconnect.com/content/maney**

SUBSCRIPTION INFORMATION

Volume 1 (2006), 4 issues per year
Print ISSN: 1748-9237 Online ISSN: 1748-9245
Individual rate: £76.00/US$141.00
Institutional rate: £235.00/US$435.00
Online-only institutional rate: £199.00/US$367.00
For special IOM^3 member rates please email **subscriptions@maney.co.uk**

For further information please contact:
Maney Publishing UK
Tel: +44 (0)113 249 7481 Fax: +44 (0)113 248 6983 Email: subscriptions@maney.co.uk
or
Maney Publishing North America
Tel (toll free): 866 297 5154 Fax: 617 354 6875 Email: maney@maneyusa.com

For further information or to subscribe online please visit
www.maney.co.uk